Vessel Extraction and Analysis of Aortic Dissection

Hui Fang[1,2], Zhanqiang Guo[1,2], Guozhu Shao[3], Zimeng Tan[1,2], Jinyang Yu[1,2], Jia Liu[3], Yukun Cao[3], Jie Zhou[1,2], Heshui Shi[3], and Jianjiang Feng[1,2(✉)]

[1] Department of Automation, Tsinghua University, Beijing, China
jfeng@tsinghua.edu.cn
[2] Beijing National Research Center for Information Science and Technology, Beijing, China
[3] Department of Radiology, Union Hospital, Tongji Medical College, Huazhong University of Science and Technology, Wuhan, China

Abstract. Aortic dissection (AD) is a dangerous disease usually diagnosed by computed tomography angiography. Segmentation of true and false lumens of aortic trunk and major branches is very important for the diagnosis and treatment of this disease. In this paper, we proposed a fully automatic vessel analysis algorithm for dissected aorta, which can output centerlines, true lumen, and false lumen of trunk and major branches, and perfusion source of branches. In our experiment, the mean dice similarity coefficient (DSC) of true lumen segmentation was 0.939 for trunk and 0.912 for branch while the mean DSC of whole lumen segmentation was 0.974 for trunk and 0.937 for branch, and the classification accuracy of branch perfusion source was 0.863.

Keywords: Aortic dissection · Centerline extraction · Lumen segmentation · Branch perfusion source

1 Introduction

Aortic dissection (AD) is a life-threatening vascular disease, which occurs by disruption of the intima along the aortic wall, resulting in separation of a true lumen (TL) and a false lumen (FL) by the intimal flap. During AD surgical planning, it is crucial to select and place the stent-graft based on the geometrical characteristics of the patient's aorta, such as lumen diameters [1,2]. CT is the standard reference for AD imaging. Manual segmentation of dissected aorta and branches from CT volumes is tedious and time-consuming [1], making automatic algorithms very desirable. However, vessel extraction of AD is a quiet challenging task because of the thin intimal flap and irregular shape changes and large intensity variations between true and false lumen [1].

Earlier studies empirically designed segmentation algorithms by considering special shape and intensity of dissected aorta. Kovács et al. [3] proposed a multi-stage method for AD segmentation, which consisted of segmentation of the aorta,

This work was supported in part by the National Natural Science Foundation of China under Grants 61976121 and 82071921.

E. Puyol Antón et al. (Eds.): STACOM 2021, LNCS 13131, pp. 48–56, 2022.
https://doi.org/10.1007/978-3-030-93722-5_6

detection of the intimal flap on the 2D cross-sections and recognition of the true and false lumens. Lee et al. [4] proposed a multi-stage method using wavelet analysis, whose core was to find the intimal flap through edge detection on the 2D cross-sections. These earlier studies have some limitations: (1) extracted 3D model is incomplete (lack of semantic branches), (2) the algorithm is not robust to noise and challenging cases, (3) evaluation is usually based on a very small number of samples, and (4) some methods are not fully automatic.

In recent years, deep CNNs have achieved the state-of-the-art results on many medical image segmentation tasks [5,6]. Researchers have started developing deep learning based segmentation algorithms for aorta dissection. Li et al. [7] used two cascaded convolutional networks to extract the adventitia and intima contours of aortic trunk. Hahn et al. [8] developed a five-step segmentation pipeline that segments the true and false lumens of aortic trunk based on centerline. Cao et al. [9] designed two U-net: the first was used for coarse aortic trunk segmentation while the second was used for fine segmentation of aortic trunk. However, none of these recent studies [7–11] tackled the problem of branch segmentation, semantic labeling, and perfusion source analysis.

We proposed a fully automatic and comprehensive vessel analysis algorithm for aortic dissection, which can perform centerline extraction, lumen segmentation of aortic trunk and nine main branches, and branch perfusion source classification. Experiments showed that the mean dice similarity coefficient (DSC) of true lumen segmentation was 0.939 for trunk and 0.912 for branch while the mean DSC of whole lumen was 0.974 for trunk and 0.937 for branch, and the classification accuracy of branch perfusion source was 0.863. Besides, as far as we know, this is the first work for lumen segmentation and perfusion source classification of AD branches using deep learning.

2 Methodology

Our scheme (see Fig. 1) is divided into three stages. The first stage is to extract centerline of aortic trunk and branches, while the second stage is to obtain true and false lumens of aortic trunk and branches with the help of the centerline, and the last stage is to determine the branch perfusion source. These steps are introduced in detail in the following three sections respectively.

2.1 Centerline Extraction

Nine main branches are considered in our study, including right common carotid artery, left common carotid artery, left subclavian artery, celiac trunk, superior mesenteric artery, two renal arteries and two iliac arteries. We take several points to represent centerline to simplify centerline extraction. This simplification is not only resistant to noise, but also beneficial to aorta image reconstruction.

For the aortic trunk, we define the centerline as 40 equidistant points. We implement landmark detection method [12] to output heat map with 40 channels, then obtain the centerline by connecting detected points (see Fig. 2).

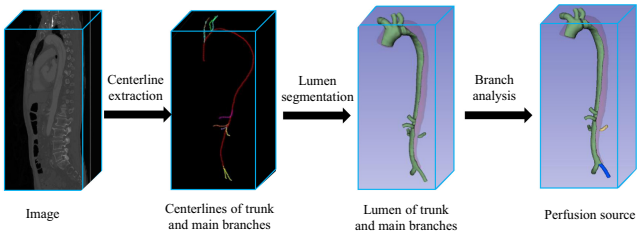

Fig. 1. Flowchart of the proposed system. The centerlines of different branches are marked by different colors and green represents true lumen while dark red represents false lumen. In the fourth image, green, yellow and blue indicates that the branch perfusion source is true lumen, false lumen and both of them respectively. (Color figure online)

Detection of branch centerline is more challenging because of the different number and length of branches for different people. To simplify the problem, nine main branches are selected and cut into fixed length, and then nine mean centerlines are calculated relative to their starting point. The mean centerline on the training dataset is defined in Eq. (1), where i represents the branch label and the branch centerline is defined as 5 equidistant points.

$$M^i = \frac{1}{N} \sum_{dataset} [0, c_2 - c_1, c_3 - c_1, c_4 - c_1, c_5 - c_1]^i \tag{1}$$

Our branch centerline extraction algorithm is divided into three steps: (1) Jointly extract the branch label and the starting point of nine branches by implementing landmark detection method [12]. (2) Calculate the initial branch centerline ($initC^i = c_0^i + M^i$) based on the predicted starting point and the mean centerline corresponding to the predicted label. (3) Fine-tune the branch centerline based on local information through the finetuning network (see Fig. 2), whose output is the centerline coordinate deviation ($\Delta x^i = C_{GT}^i - initC^i$).

2.2 Lumen Segmentation

Our lumen segmentation method takes a local volume along the centerline as input and outputs the whole lumen mask and the true lumen mask. False lumen can be simply obtained by subtracting the true lumen from the whole lumen.

Data Preprocessing. Firstly, all image resolutions are resized to 1 mm. Based on a centerline composed of several key points, rotation and cropping are used to reconstruct aortic vessel image orthogonal to local centerline, which is similar to the multiplanar reformation (MPR). The dimension of reconstructed image is $64 \times 64 \times L$ for trunk and $32 \times 32 \times L$ for branch, where L represents the distance between two adjacent points. Then 3D lumen segmentation takes these reconstructed image blocks as input.

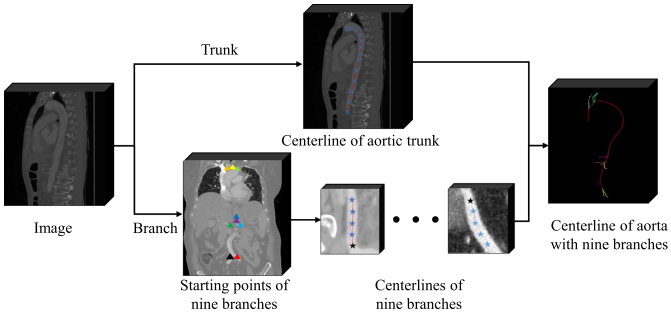

(a) Flowchart of centerline extraction

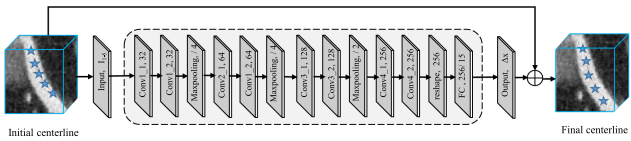

(b) Branch centerline finetuning network

Fig. 2. Flowchart of centerline extraction. (a) The trunk centerline is directly obtained by landmark detection method. The branches starting points are obtained by landmark detection, and then fine-tune the branch centerline by network. (b) The input of fine-tuning network is a 5-channel image with a size of $32 \times 32 \times 32$, where each channel image is centered on the corresponding point of the initial centerline. The output of the network is a 15-dimensional vector represents the centerline coordinate deviation.

Network. Considering the anisotropy of the reconstructed image, that is, the amount of information between Z-axis and XY-axis is different, 3D flat U-net for lumen segmentation called FU-net is designed (see Fig. 3). Different from traditional U-net, FU-net retains the Z-axis resolution during down-sampling, whose advantage is to improve the segmentation accuracy in XY plane while considering the continuity of the Z-axis.

Loss Function. Dice loss function and deep supervision are used in the lumen segmentation experiment. The final loss function is defined as follows, where the subscript of loss represents the resolution.

$$LOSS = loss_1 + 0.6 \times loss_{\frac{1}{2}} + 0.3 \times loss_{\frac{1}{4}} + 0.1 \times loss_{\frac{1}{8}}. \tag{2}$$

2.3 Branch Perfusion Source Classification

The application of endovascular repair of aortic dissection is different for patients with different branch perfusion sources. Therefore, the classification of perfusion source is of great significance in clinical practice. There are three types of branch perfusion sources, true lumen, false lumen, or both of them, the latter two of which are abnormal branches. The ground truth of category labels can be simply

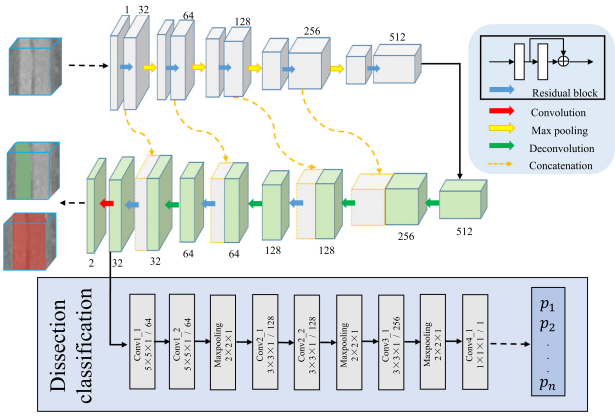

Fig. 3. Lumen segmentation and dissection classification network structure. The resolution of Z-axis remains the same in the segmentation part, which means after max-pooling layer, the size changes from (x, y, z) to $(x/2, y/2, z)$. The output of dissection classification network is a column vector whose length is equal to the length of the Z-axis of the input image.

obtained by comparison of true lumen and whole lumen masks. Our classification algorithm is divided into two steps. First, a dissection classification network is used to determine whether the branch comes from both lumens. It is built based on segmentation network since they are quite related tasks (see Fig. 3). In the second stage, we exploit the distance difference to determine whether the branch comes from false lumen. If the distance of a branch from true lumen of trunk is 3 mm greater than the distance from the whole lumen of trunk, its perfusion source is attributed to false lumen.

3 Experiment

Data. We collected 255 contrast-enhanced AD CT from 255 different patients with type A dissection (97 patients) or type B dissection (158 patients). The size of volume is $512 \times 512 \times Z(389 - 1479)$. Firstly, we discarded 36 CT volumes with low contrast. Then the branch perfusion source of the remaining 219 CT volumes was labeled by an experienced doctor. 100 of them (49 type A and 51 type B) were manually labeled with vessel centerlines, and the whole lumen and true lumen of the aorta and nine main branches with 3D slicer (https://www.slicer.org/). The voxel spacing of all images was resized to 1 mm. 100 CT volumes with manually labeled vascular lumens were randomly divided into training set (60) and test set (40). The test set was increased to 159 when evaluating the branch perfusion source classification performance. To improve the robustness of our model, training images are augmented by flip transform, rotation transform and the combination of them.

Table 1. Comparison of aortic lumen segmentation performance in the reconstruction space, where the evaluation standard is dice similarity coefficient (DSC), and the number in brackets represents the standard deviation.

		Method	DSC	Precision	Recall
Trunk	Whole lumen	Li et al. [7]	0.960(0.009)	0.952(0.017)	0.967(0.012)
		FU-net	**0.974(0.009)**	**0.978(0.012)**	**0.970(0.019)**
	True lumen	Li et al. [7]	0.891(0.026)	0.895(0.040)	0.887(0.026)
		FU-net	**0.939(0.032)**	**0.942(0.034)**	**0.937(0.035)**
Branch	Whole lumen	FU-net	0.937(0.024)	0.929(0.029)	0.946(0.026)
	True lumen	FU-net	0.912(0.051)	0.920(0.038)	0.907(0.074)

Table 2. Comparison of the results of true lumen segmentation of the entire aorta with branches in the original coordinate space. In other methods, it is difficult to separate the trunk and branches. In addition, true lumen segmentation is more challenging and more clinically meaningful.

Method	DSC	Precision	Recall
2D U-net [5]	0.812(0.103)	0.847(0.066)	0.790(0.127)
3D U-net [6]	0.833(0.051)	0.832(0.060)	0.840(0.077)
3D V-net [13]	0.809(0.099)	0.810(0.091)	0.821(0.126)
FU-net	**0.907(0.027)**	**0.906(0.028)**	**0.908(0.034)**

Results. We reproduced the algorithm in Li et al. [7] which can segment only the aortic trunk. In addition, we compared our algorithm with 2D U-net [5], 3D U-net [6], and 3D V-net [13], because (1) these networks have good generalization, (2) recent AD segmentation algorithms [8–10] are based on these networks, and (3) open source implementations are available.

Firstly, we compared our method with Li et al. [7] in the reconstruction space, namely, aligned to local centerline (see Table 1). Furthermore, we mapped the result of our segmentation algorithm back to the original coordinate space and compared with segmentation algorithms without utilizing centerline information (see Table 2).

In Table 1, the average DSC for FU-net was 0.939 for trunk and 0.912 for branch on the task of true lumen segmentation. The score is higher than [7], which demonstrated that it is helpful to add 3D information in lumen segmentation. In the original coordinate space (see Table 2), the average DSC of our proposed method was at least 7% higher than those algorithms without utilizing centerline information, which proved that the mutil-stage method we designed is effective.

Figure 4 shows the 3D meshes of the segmentation results of four algorithms and the comparison between our method and 3D U-net in sagittal view in the original coordinate space. Compared to our method, other algorithms have some

problems such as the disconnection of blood vessels and the confusion of true and false lumen.

Table 3. Confusion matrix of the classification task of branch perfusion sources.

Label	Predict				
	True lumen	False lumen	Both	Total	Recall
True lumen	970	122	38	1130	0.858
False lumen	15	95	2	112	0.848
Both	12	7	170	189	0.899

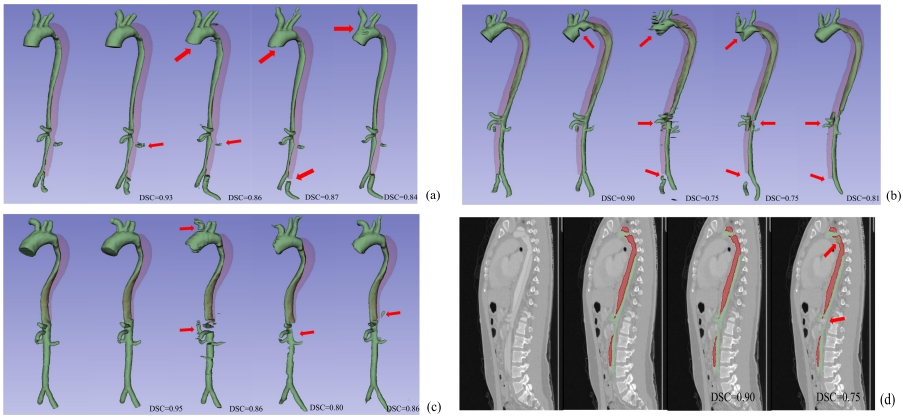

Fig. 4. In (a) (b) (c), which represent three different samples, from left to right are 3D meshes of the ground truth, ours, 2D U-net, 3D U-net and 3D V-net. In sagittal view (d), from left to right are original image, ground truth, ours and 3D U-net. Note that green represents true lumen while dark red represents false lumen, and the red arrow marks the poor segmentation part. Dice scores are shown below. (Color figure online)

Table 3 shows the confusion matrix of the classification task of branch perfusion sources. The average classification accuracy is 0.863. Misclassification usually occurs in difficult samples such as calcification and thrombosis. In the task of judging whether a branch arises from false lumen, the performance of our algorithm is not ideal, indicating that other criteria need to be added in addition to distance.

4 Conclusion

In this paper, we proposed an automatic vascular extraction algorithm for CT of aortic dissection, which can obtain centerlines, true lumen, and false lumen of

trunk and major branches, and can estimate the perfusion source of branches. To our knowledge, it is the most comprehensive vessel analysis algorithm for AD in the public literature. However, our current method still has two shortcomings. One is that the variation of branch topology is not considered (although uncommon), and the other is that the lumen segmentation result at the bifurcation point is not accurate enough. We intend to overcome them in the future.

References

1. Pepe, A., et al.: Detection, segmentation, simulation and visualization of aortic dissections: a review. Med. Image Anal. **65**, 101773 (2020)
2. Chiesa, R., Melissano, G., Zangrillo, A., Coselli, J.S.: Thoraco-Abdominal Aorta: Surgical and Anesthetic Management, vol. 783. Springer, Milano (2011). https://doi.org/10.1007/978-88-470-1857-0
3. Kovács, T., Cattin, P., Alkadhi, H., Wildermuth, S., Székely, G.: Automatic segmentation of the aortic dissection membrane from 3D CTA images. In: Yang, G.-Z., Jiang, T.Z., Shen, D., Gu, L., Yang, J. (eds.) MIAR 2006. LNCS, vol. 4091, pp. 317–324. Springer, Heidelberg (2006). https://doi.org/10.1007/11812715_40
4. Lee, N., Tek, H., Laine, A.F.: True-false lumen segmentation of aortic dissection using multi-scale wavelet analysis and generative-discriminative model matching. In: Medical Imaging 2008: Computer-Aided Diagnosis, vol. 6915, p. 69152V. International Society for Optics and Photonics (2008)
5. Ronneberger, O., Fischer, P., Brox, T.: U-net: convolutional networks for biomedical image segmentation. In: Navab, N., Hornegger, J., Wells, W.M., Frangi, A.F. (eds.) MICCAI 2015. LNCS, vol. 9351, pp. 234–241. Springer, Cham (2015). https://doi.org/10.1007/978-3-319-24574-4_28
6. Çiçek, Ö., Abdulkadir, A., Lienkamp, S.S., Brox, T., Ronneberger, O.: 3D U-net: learning dense volumetric segmentation from sparse annotation. In: Ourselin, S., Joskowicz, L., Sabuncu, M.R., Unal, G., Wells, W. (eds.) MICCAI 2016. LNCS, vol. 9901, pp. 424–432. Springer, Cham (2016). https://doi.org/10.1007/978-3-319-46723-8_49
7. Li, Z., et al.: Lumen segmentation of aortic dissection with cascaded convolutional network. In: Pop, M., et al. (eds.) STACOM 2018. LNCS, vol. 11395, pp. 122–130. Springer, Cham (2019). https://doi.org/10.1007/978-3-030-12029-0_14
8. Hahn, L.D., et al.: CT-based true-and false-lumen segmentation in type B aortic dissection using machine learning. Radiol. Cardiothorac. Imaging **2**(3), e190179 (2020)
9. Cao, L., et al.: Fully automatic segmentation of type B aortic dissection from CTA images enabled by deep learning. Eur. J. Radiol. **121**, 108713 (2019)
10. Fantazzini, A., et al.: 3D automatic segmentation of aortic computed tomography angiography combining multi-view 2D convolutional neural networks. Cardiovasc. Eng. Technol. **11**(5), 576–586 (2020)
11. Xu, X., He, Z., Niu, K., Zhang, Y., Tang, H., Tan, L.: An automatic detection scheme of acute stanford type A aortic dissection based on DCNNs in CTA images. In: Proceedings of the 2019 4th International Conference on Multimedia Systems and Signal Processing, pp. 16–20 (2019)

12. Tan, Z., Duan, Y., Wu, Z., Feng, J., Zhou, J.: A cascade regression model for anatomical landmark detection. In: STACOM 2019. LNCS, vol. 12009, pp. 43–51. Springer, Cham (2020). https://doi.org/10.1007/978-3-030-39074-7_5
13. Milletari, F., Navab, N., Ahmadi, S.-A.: V-net: fully convolutional neural networks for volumetric medical image segmentation. In: 2016 Fourth International Conference on 3D Vision (3DV), pp. 565–571. IEEE (2016)